Generation of few-cycle laser pulses: Comparison between atomic and molecular gases in a hollow-core fiber*

Zhi-Yuan Huang(黄志远)[1,2], Ye Dai(戴晔)[1], Rui-Rui Zhao(赵睿睿)[2], Ding Wang(王丁)[2,†], and Yu-Xin Leng(冷雨欣)[2,‡]

[1] *Department of Physics, Shanghai University, Shanghai* 200444, *China*

[2] *State Key Laboratory of High Field Laser Physics, Shanghai Institute of Optics and Fine Mechanics, Chinese Academy of Sciences, Shanghai* 201800, *China*

(Received 11 December 2015; revised manuscript received 29 February 2016; published online 31 May 2016)

We numerically study the pulse compression approaches based on atomic or molecular gases in a hollow-core fiber. From the perspective of self-phase modulation (SPM), we give the extensive study of the SPM influence on a probe pulse with molecular phase modulation (MPM) effect. By comparing the two compression methods, we summarize their advantages and drawbacks to obtain the few-cycle pulses with micro- or millijoule energies. It is also shown that the double pump-probe approach can be used as a tunable dual-color source by adjusting the time delay between pump and probe pulses to proper values.

Keywords: hollow-core fiber, phase modulation, pulses compression, few-cycle pulses

PACS: 42.65.–k, 42.65.Re, 42.65.Jx, 42.81.Qb **DOI:** 10.1088/1674-1056/25/7/074205

1. Introduction

Ultrashort laser pulses with duration of only a few optical cycles possess extensive applications in various fields such as light-matter interactions, high-order harmonic generation (HHG),[1] attosecond physics,[2,3] atomic and molecular physics.[4–6] A popular pulse compression scheme is allowing the pulses to propagate through a hollow-core fiber (HCF) filled with atomic gases.[7,8] The temporal self-phase modulation (SPM) created by the electronic Kerr nonlinearity gives rise to spectral broadening and imparts a positive chirp on pulses that can then be compensated by using the chirped mirrors, which generates the few-cycle pulses with micro- or millijoule energies.[9–13] However, since SPM is a third-order nonlinear process and the induced time-dependent phase is proportional to the pulse intensity, when this pulse compression technique is applied to the high intensity region, the phase behavior becomes much more complicated, and its complete compensation is impractical. Moreover, the spectral profile of generated few-cycle pulses exhibits a multipeak structure, and its central wavelength is limited to a narrow range around the fundamental wavelength of 800 nm.

An alternative method to obtain the few-cycle pulses termed molecular phase modulation (MPM) has been presented.[14–17] In comparison with atomic gases, when molecular gases interact with an intense pump pulse, the molecular alignment revivals are created. Then the molecular alignment produces a strong phase modulation on the time-delay probe pulse, which achieves the frequency tuning and spectral broadening.[18–23] In the process of spectral broadening, the MPM effect imparts a near-linear positive or negative chirp on the probe pulse by tuning the time delay between pump and probe pulses, it means that the probe pulse can be compensated by the common glasses instead of chirped mirrors. With this pump-probe configuration, we can obtain the frequency-tunable few-cycle pulses, which is very promising as a tunable source. However, this approach is restricted by the intensity of the probe pulse; the intense pulse will enhance the nonlinear effects such as SPM effect which induces a disruptive spectral modulation.

In our previous work,[24,25] we first achieved several hundred nanometers wavelength tuning by using the double pump pulses and then particularly studied the process of frequency tuning and spectral broadening based on MPM effect. In this work, seen from the SPM perspective, we review the process and specifically investigate the extensive influence of SPM effect on the probe pulse with MPM effect. In addition, we make a comparison between atomic and molecular gases for generating the few-cycle pulses and discuss the advantages and limitations of these two methods. Furthermore, using the double pump-probe approach, we can simultaneously obtain the two few-cycle pulses with different spectral ranges.

*Project supported by the National Natural Science Foundation of China (Grant Nos. 11204328, 61221064, 61078037, 11127901, 11134010, and 61205208), the National Basic Research Program of China (Grant No. 2011CB808101), and the Natural Science Foundation of Shanghai, China (Grant No. 13ZR1414800).

†Corresponding author. E-mail: wangding@siom.ac.cn

‡Corresponding author. E-mail: lengyuxin@siom.ac.cn

© 2016 Chinese Physical Society and IOP Publishing Ltd

2. SPM effect based on atomic gases

The pulse propagation equation based on the atomic-gases-filled HCF can be expressed as[26–28]

$$(\partial_z - \mathrm{i}\hat{L})E = \mathrm{i}\hat{T}\left[\frac{\omega_0}{c}n_2 h|E|^2 E\right] - \frac{\sigma}{2}\mathrm{d}E - \frac{1}{2}\frac{f}{I}E - \frac{\mathrm{i}q_\mathrm{e}^2}{2c\omega_0 m_\mathrm{e}\varepsilon_0}\hat{T}^{-1}[\mathrm{d}E], \quad (1)$$

where the pulse envelope E is normalized to the intensity I; the constants c, σ, q_e, m_e, ε_0, and n_2 are light speed in vacuum, impact ionization cross section, electron charge and mass, vacuum permittivity, and instantaneous Kerr nonlinear refractive index, respectively. The linear operator $\hat{L} = \mathrm{i}\alpha^{(0)} - \alpha^{(1)}\partial_\tau + \sum_{m=2}^{\infty}(\mathrm{i}\partial_\tau)^m\left[\beta^{(m)} + \mathrm{i}\alpha^{(m)}\right]/m!$ describes the waveguide mode attenuation α and the dispersion β, where $\alpha^{(m)} = \mathrm{d}^m\alpha/\mathrm{d}\omega^m|_{\omega=\omega_0}$ and $\beta^{(m)} = \mathrm{d}^m\beta/\mathrm{d}\omega^m|_{\omega=\omega_0}$; ω_0 is the central angular frequency of the pulse. The delay frame moving at the group velocity of the fundamental mode $\tau = t - \beta^{(1)}z$ is introduced. The operator $\hat{T} = 1 + (\mathrm{i}/\omega_0)\partial_\tau$ describes the self-steepening effects. The coefficients $h = \int_0^a V^4 r\mathrm{d}r/\int_0^a V^2 r\mathrm{d}r$, $d = \int_0^a \rho V^2 r\mathrm{d}r/\int_0^a V^2 r\mathrm{d}r$, and $f = \int_0^a W(\rho_\mathrm{nt} - \rho)I_\mathrm{p} r\mathrm{d}r/\int_0^a V^2 r\mathrm{d}r$ represent the Kerr, plasma and ionization effects encoded in the pulse transverse mode $V = \mathrm{J}_0(ur/a)$, where r is transverse coordinate; a is fiber inner radius; W is the ionization rate; ρ_nt is the neutral density of gas; I_p is the ionization potential; $\mathrm{J}_0(x)$ is the 0th order Bessel function of the first kind; u is the first zero point of $\mathrm{J}_0(x)$. Assuming electrons are born at rest, the electron density ρ evolves as

$$\frac{\partial\rho}{\partial t} = W(\rho_\mathrm{nt} - \rho) + \frac{\sigma}{I_\mathrm{p}}\rho I, \quad (2)$$

where the ionization rate W is calculated according to Perelomov–Popov–Terentiev (PPT) theory.[29] The pulse envelope E at the input of the HCF is written as $E(t, z=0) = f_\mathrm{coup}\sqrt{P_0/S_\mathrm{mod}}\exp\left[-(2\ln 2)t^2/\tau^2\right]$, where $P_0 = 0.94E_0/\tau$ is initial peak power, E_0 is the input pulse energy, τ is the pulse full width at half maximum (FWHM); $S_\mathrm{mod} = 0.5\pi w_0^2$ is the fundamental mode area, w_0 is the $1/e^2$ radius of the beam intensity Gaussian profile at the focus just before the input of HCF; f_coup is the fraction of the pulse that is coupled to the fundamental mode. When $w_0 = 0.65a$, about 98% of the pulse energy is coupled to the fundamental mode, which corresponds to $f_\mathrm{coup} \cong 0.88$.[30]

In this work, we employ 1-m HCF with 250-μm inner diameter. The initial Gaussian pulse is 40-fs FWHM with central wavelength 800 nm. The HCF compressor filled with noble gas is a widely used technique to obtain the few-cycle pulses with micro- or millijoule energies. Usually, considering the conditions of input pulse energy and gas pressure, we will choose the different gases to broaden spectrum. Table 1 shows the ionization potential and nonlinear refractive index for Kr, Ar, and Ne gases with pressure 1 bar at 800 nm. Since Kr gas possesses the high nonlinear refractive index, even though the pulse energy and gas pressure are low, the pulse spectrum can be broadened effectively. But for intense pulse energy, we usually use Ne gas to compress the pulse due to its high ionization potential. Ar gas is a suitable choice between these two cases.

Table 1. The ionization potential and nonlinear refractive index of noble gases at 800 nm for the pressure of 1 bar.

Gas type	Ionization potential/eV	Nonlinear refractive index n_2 /cm^2·W^{-1}
Kr	13.99961	2.78×10^{-19}
Ar	15.75962	1.00×10^{-19}
Ne	21.56460	7.50×10^{-21}

Here, we use the root-mean-square (RMS) method to express the spectral broadening, and the broadening factor is defied.[25,31,32] As shown in Fig. 1(a), the spectral width for input pulse energy 0.05 mJ increases with respect to Kr gas pressures from 0.1 bar to 1.0 bar, and exhibits a linear relation. Figure 1(b) shows the temporal intensities of the output (blue solid curves) and compressed pulses with group delay dispersion (GDD, red solid curves) or GDD, third-order dispersion (TOD, black-dotted curves) compensation at gas pressure 0.5 bar. The compressed pulse FWHM is 10.0 fs after -70 fs^2 and 81 fs^3 compensation. We can observe that the TOD compensation improves the pulse leading edge, but it has little influence on pulse duration (ΔFWHM < 0.2 fs) in Fig. 1(d). In Fig. 1(f), when the gas pressure is increased to 0.8 bar, the output pulse spectrum (green solid curves) is extended to a three-peak structure and possesses the greater frequency chirp compared to Fig. 1(c). Thus the pulse duration is compressed to 7.2 fs with -64 fs^2 and 49 fs^3 compensation, which is close to the Fourier transform limit (FTL) 7.0 fs.

Figures 2(a) and 2(b) show the temporal and spectral profiles of the compressed pulse with input energy 0.2 mJ for Ar gas pressure 1.0 bar, respectively. In Fig. 2(b), we can notice the pulse spectrum is broadened effectively (green solid curves) and the phase with positive chirp (blue solid curves) is compensated obviously (yellow-dotted curves). As shown in Fig. 2(a), after -41 fs^2 and 26 fs^3 compensation, a near-single-cycle pulse with FWHM 3.8 fs equaling to FTL is obtained. For intense pulse with energy 1.0 mJ, we use Ne gas to achieve the spectral broadening at gas pressure 1.5 bar, and the compressed pulse duration is 6.6 fs with -55 fs^2 and 45 fs^3 compensation in Figs. 2(c) and 2(d). With such high energy, the pulse undergoes the strong nonlinear effects such as plasma effect. Figures 3(a) and 3(b) show the temporal and spectral intensities of output pulse with (blue solid curves) or without (red solid curves) plasma effect. We can observe the pulse presents an oscillation located in its roof due to the plasma effect. In Figs. 3(c)–3(e), it is found that the peak intensity of the pulse decreases more quickly, with the proportion decreasing from 1.0 to 0.8, the temporal profile begins to split around 0.8 m, and a larger spectral modulation is survived in its spectrum compared to Figs. 3(f)–3(h) for switching off the plasma effect.

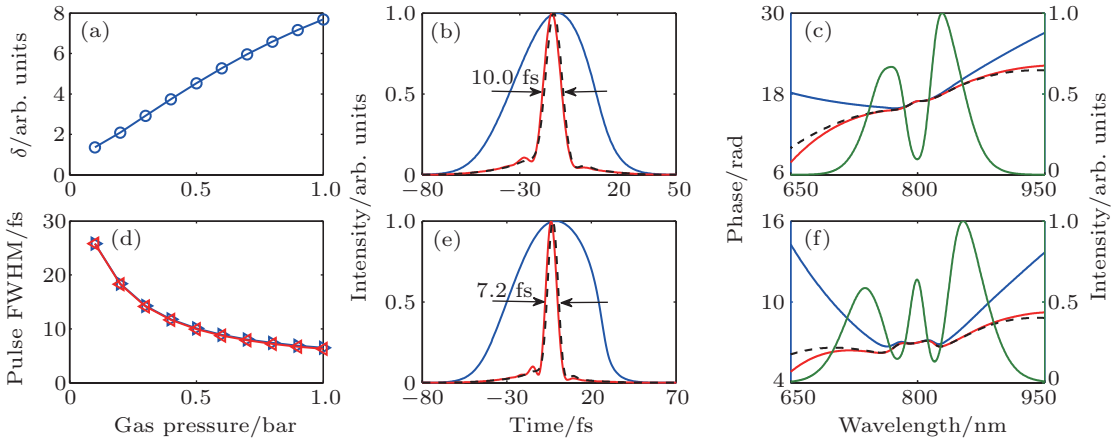


Fig. 1. (color online) (a) and (d) The spectral broadening factor (blue circle lines) and the pulse FWHM only using GDD (blue right triangle lines) or GDD, TOD (red left triangle lines) compensation of the compressed pulses with different gas pressures. (b) and (e) The temporal profiles of output pulses (blue solid lines), compressed pulses with GDD (red solid lines) or GDD, TOD compensation (black-dotted lines) for various gas pressures 0.5 bar and 0.8 bar, respectively. (c) and (f) The corresponding spectral intensities (green solid lines) and phase.

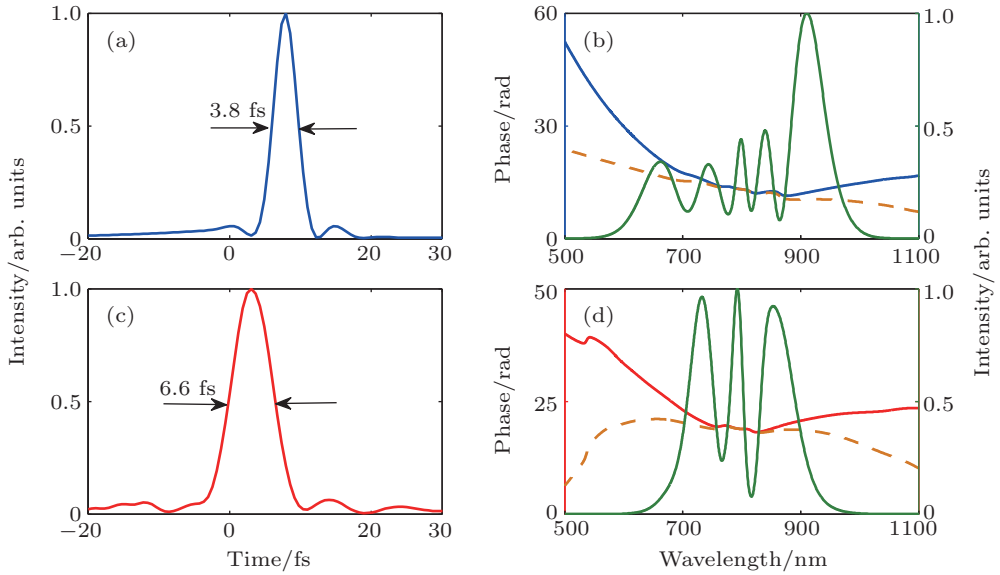


Fig. 2. (color online) (a) and (c) The temporal intensities of compressed pulses. (b) and (d) The spectral intensities (green solid lines), the phase before (blue and red solid lines) and after (yellow-dotted lines) compensation. Panels (a)–(b) and (c)–(d) correspond to argon and neon gases, respectively.

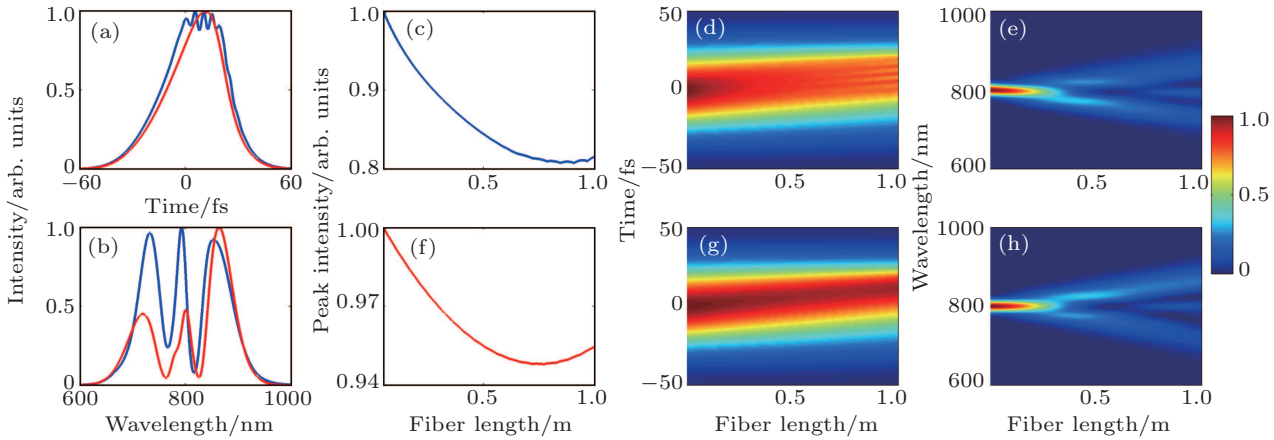


Fig. 3. (color online) (a) and (b) The temporal and spectral profiles of output pulses with (blue solid lines) or without (red solid lines) considering plasma effect. Panels (c) and (f), (d) and (g), (e) and (h) represent the evolutions of peak intensity, time and frequency domains of the pulse with different fiber lengths, respectively. Panels (c)–(e) and (f)–(h) with or without plasma effect.

3. MPM and SPM effects based on molecular gases

The pulse propagation dynamics in molecular gases can be described as

$$\begin{aligned}&(\partial_z - \mathrm{i}\hat{L})E \\ &= \mathrm{i}\hat{T}\left[\frac{\omega_0}{c}n_2 h|E|^2 E\right] - \frac{\sigma}{2}\mathrm{d}E \\ &\quad - \frac{1}{2}\frac{f}{I}E - \frac{\mathrm{i}q_\mathrm{e}^2}{2c\omega_0 m_\mathrm{e}\varepsilon_0}\hat{T}^{-1}[\mathrm{d}E] + \mathrm{i}\frac{\omega_0}{\mathrm{c}}\hat{T}[\delta n_\mathrm{rot}E], \quad (3)\end{aligned}$$

where the last term on the right-hand side from Eq. (3) is the only difference compared with Eq. (1). The $\delta n_\mathrm{rot} = \int_0^a \Delta n V^2 r\mathrm{d}r / \int_0^a V^2 r\mathrm{d}r$ represents the effect of change of refractive index Δn created by molecular rotation effect, where $\Delta n(t,r,z) = 2\pi(\rho_\mathrm{nt}\Delta\alpha/n_0)[\langle\langle\cos^2\theta\rangle\rangle(t,r,z) - 1/3]$,[33] $\Delta\alpha$ is the polarizability difference between parallel to and perpendicular to the molecular axis; n_0 is the linear refractive index; the molecular alignment is averaged over the Boltzmann distribution and expressed as[34]

$$\begin{aligned}\langle\langle\cos^2\theta\rangle\rangle &= \sum_J \frac{g_J \exp[-\varepsilon_J/kT]}{Q} \\ &\quad \times \sum_{M=-J}^{J} \langle\psi_{J,M}|\cos^2\theta|\psi_{J,M}\rangle, \quad (4)\end{aligned}$$

where g_J factor reflects the nuclear spin statistics of the molecule; Q is the rotational partition function; k is the Boltzmann constant; T is the molecular rotational temperature; $\psi_{J,M}$ is the rotational wave function of the evolved molecules. The $\varepsilon_J = B_0 J(J+1) - D_0 J^2(J+1)^2$ where B_0 is the rotational constant; D_0 is the centrifugal distortion constant; J is the angular quantum number. The alignment-induced ionization rate is also introduced in Eq. (2) by a modulation factor $\eta = 1 + (1.5a_2 - 3.75a_4)(\langle\langle\cos^2\theta\rangle\rangle - 1/3) + 4.375a_4(\langle\langle\cos^4\theta\rangle\rangle - 1/5)$ on W where $a_2 = 0.39$ and $a_4 = -0.21$.[35]

Here, we use molecular nitrogen at gas pressure 1.0 bar and employ the 1800-nm, 1.3-mJ, 90-fs pump pulse and 800-nm, 0.05-mJ, 40-fs probe pulse. Figures 4(a) and 4(c) show the blueshifts and redshifts for various time delays with (blue up triangle curves) or without (red down triangle curves) considering SPM effect, respectively. With increasing the time delays, we can see the wavelength shifts of probe pulses are first enhanced and then suppressed whether the SPM effect is considered or not. In Figs. 4(b) and 4(d), we present the spectral broadening factor of the output probe pulses with (green circle curves) or without (yellow square curves) SPM. The simulation results show the spectral width displays the opposite behavior compared to the wavelength shift. It is also shown that the SPM effect plays a significant role in the process of spectral broadening. For SPM, it imparts a positive chirp on the probe pulse; while for MPM, it can allow a negative or positive chirp by tuning the time delay. Therefore, when the time delay is tuned to the positive interval, the spectral broadening will be enhanced due to SPM effect; but for the negative interval, it will be suppressed because of the balance between the positive chirp from SPM and the negative chirp induced by MPM. Based on this analysis, as shown in Fig. 4(b), we can conclude that the MPM first imparts a positive chirp and then a negative chirp on the probe pulse. In Fig. 4(d), we can also observe the positive and negative chirp induced by MPM, but the curves reflect the opposite result compared to Fig. 4(b).

Figures 5(a), 5(e) and 5(b), 5(f) show the evolutions of wavelength shift and broadening factor along 1-m fiber with (blue solid curves) or without (red solid curves) SPM effect for different delays 4.14 ps and 4.27 ps with 40 fs, 0.05-mJ probe pulse, respectively. As shown in Figs. 5(a) and 5(e), we

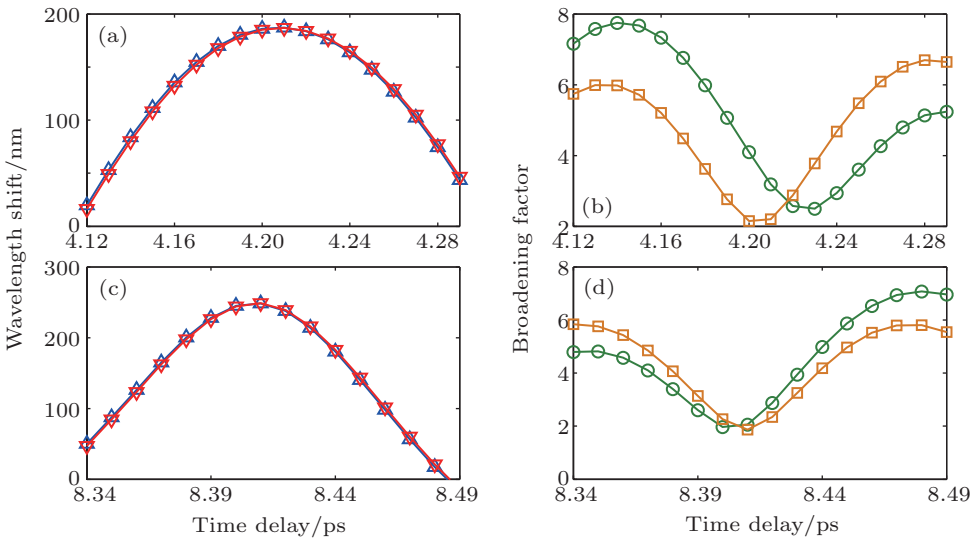


Fig. 4. (color online) (a) and (c) The wavelength shift of the probe pulses with (blue up triangle lines) or without (red down triangle lines) SPM effect. (b) and (d) The spectral broadening factor with (green circle lines) or without (yellow square lines) considering SPM effect.

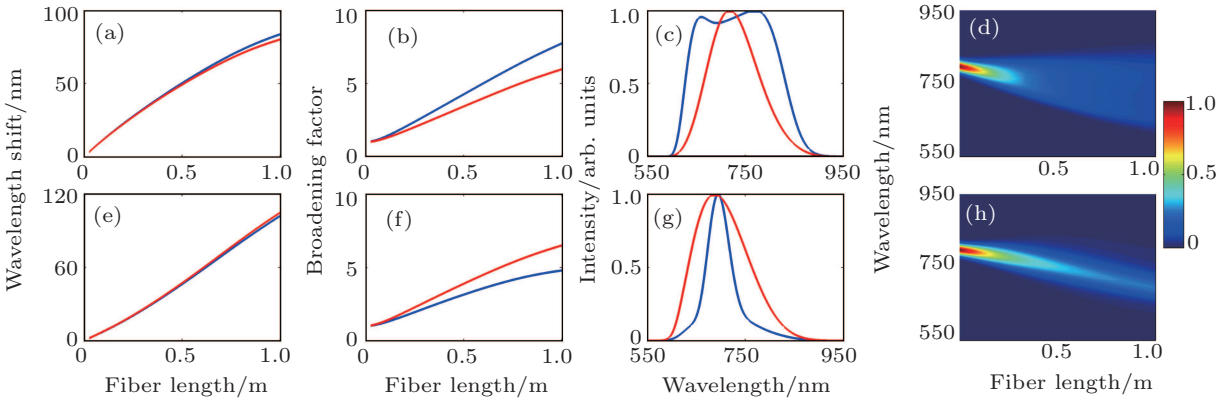


Fig. 5. (color online) (c) and (g) The spectral profiles of output pulses. (a) and (e), (b) and (f), (d) and (h), represent the evolutions of wavelength shift, broadening factor, and frequency domains for different fiber lengths, respectively. Panels (a)–(d) and (e)–(h) correspond to different delays 4.14 ps and 4.27 ps, together with (blue solid lines) or without (red solid lines) SPM effect.

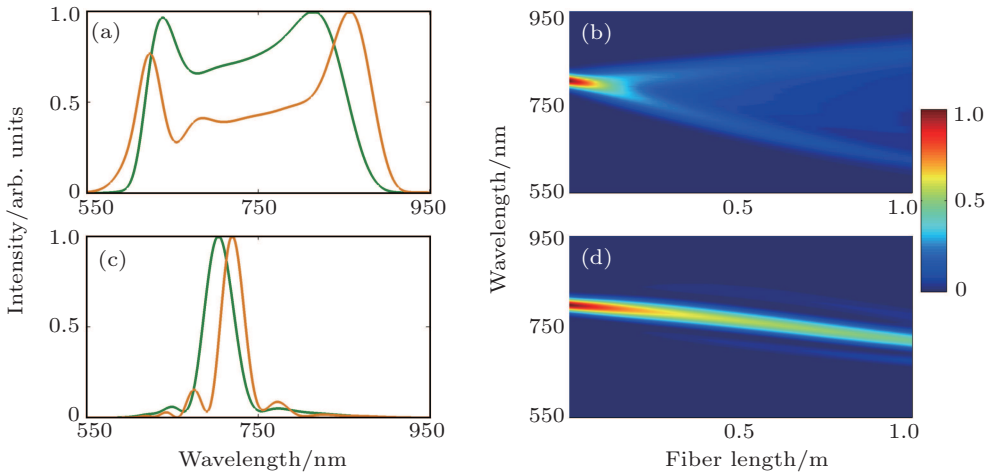


Fig. 6. (color online) (a) and (c) The spectral profiles of output pulses. (b) and (d) The evolutions of spectral intensities in HCF with initial energy 0.2 mJ. Panels (a), (b) and (c), (d) correspond to time delays 4.14 ps and 4.27 ps. Green and yellow solid lines represent different pulse energies 0.1 mJ and 0.2 mJ, respectively.

can see the wavelength shift increases nearly linearly with respect to fiber length, and the SPM has little influence on it since the frequency tuning is mainly created by molecular rotational effect. In Figs. 5(b) and 5(f), the spectral broadening also exhibits a similar trend, increasing along the fiber, but the SPM produces a positive or negative effect on the probe pulse at various delays, which results in different spectral broadening. Figures 5(c), 5(g) and 5(d), 5(h) present the spectral profiles of output pulse and the spectral evolutions in the fiber. We can clearly observe the wavelength tuning and spectral broadening of the probe pulse in HCF. However, for an intense probe pulse, the enhanced SPM will induce a large spectral modulation. Figures 6(a) and 6(c) show the output spectral intensities with different input energy 0.1 mJ (green solid curves) and 0.2 mJ (yellow solid curves) at time delays 4.14 ps and 4.27 ps, respectively. As can be seen, for positive chirp interval, the probe pulse possesses a disruptive modulation; while for negative chirp interval, the negative chirp existing in the spectrum is obviously offset due to the positive chirp from SPM. The spectral evolutions in the fiber also reflect these behaviors in Figs. 6(b) and 6(d).

Based on this pump-probe approach, we can obtain the frequency-tunable probe pulse with a negative chirp by tuning the time delay, thus the popular optical glasses are used to compensate the probe pulse. Figures 7(a) and 7(d) show the compressed pulse FWHM with increasing glass length of FK51A for different delays 4.27 ps and 8.34 ps with input probe pulse duration 40 fs, respectively. In this process, we take into account the complete dispersion compensation including GDD and higher-order of the glasses. In Figs. 7(b) and 7(e), we present the temporal intensities of the compressed probe pulses with pulse duration 7.8 fs and 9.4 fs, and correspond to the glass length 1.9 mm and 4.2 mm, respectively. The corresponding spectral profiles (green solid curves), phase before (blue and red solid curves) and after (black dotted curves) compensation are give in Figs. 7(c) and 7(f). As shown in Fig. 8, we obtain the optimal FWHM 7.7 fs and 8.5 fs only using GDD compensation with 88 fs^2 and 118 fs^2, respectively. We can notice the FWHM of the compressed pulse for delay 8.34 ps exhibits a larger difference due to the 4.2-mm glass including more high-order dispersion.

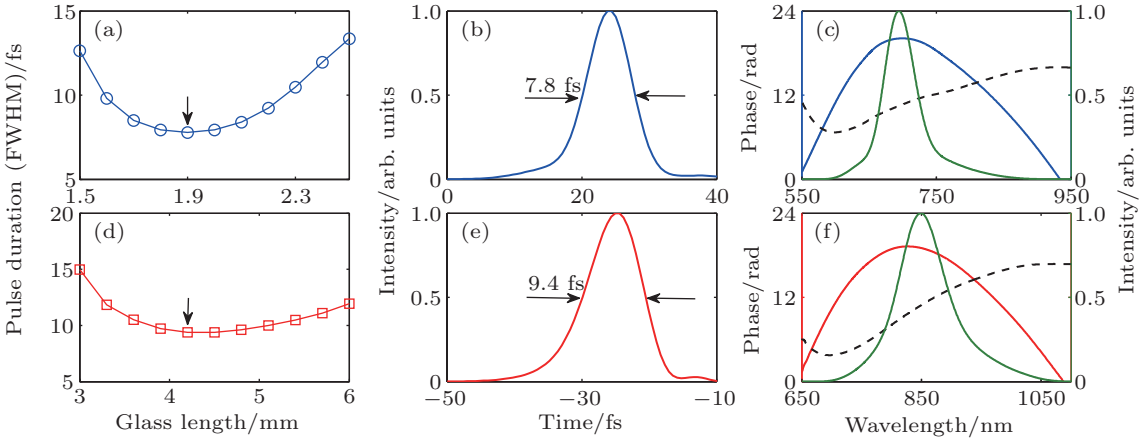


Fig. 7. (color online) (a) and (d) The probe pulses duration compensated by different glass lengths. (b) and (e) The temporal intensities of the compressed probe pulses. (c) and (f) The spectral intensities (green solid lines), the phase before (blue and red solid lines) and after (black dotted lines) compensation. Panels (a)–(c) and (d)–(f) correspond to various time delays 4.27 ps and 8.34 ps, respectively.

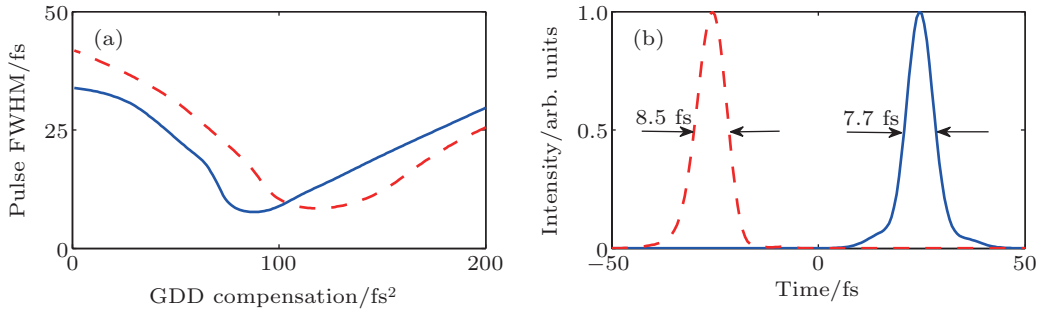


Fig. 8. (color online) (a) The probe pulses FWHM with various GDD compensation. (b) The temporal profiles of the compressed pulses. Blue solid lines and red dotted lines, represent different time delays 4.27 ps and 8.34 ps, respectively.

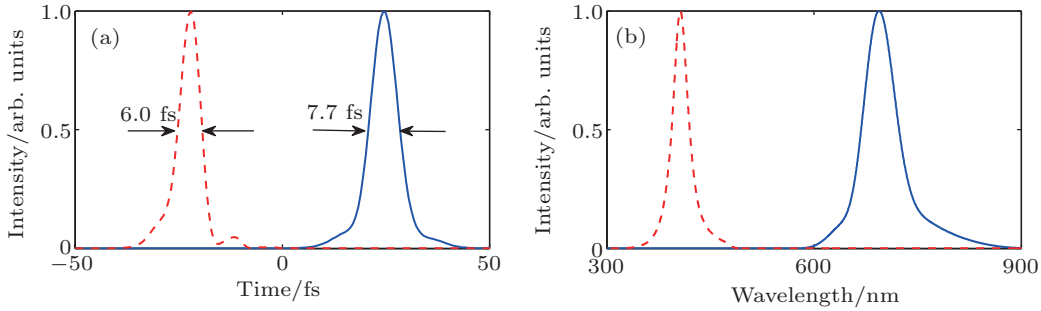


Fig. 9. (color online) (a) and (b) The temporal and spectral profiles of the compressed pulses. Blue solid lines and red dotted lines, represent the first and second probe pulses with different delays 4.27 ps and 8.40 ps at central wavelength 800 nm and 400 nm, respectively.

Figures 9(a) and 9(b) show the temporal and spectral intensities of the first (blue solid curves) and second (red dotted curves) probe pulses with initial pulse duration 40 fs for different time delays 4.27 ps and 8.40 ps, together with the central wavelength 800 nm and 400 nm, respectively. As shown in Fig. 9(a), after using 88 fs^2 and 48 fs^2 GDD compensation, the probe pulses are compressed to 7.7 fs and 6.0 fs. With the double pump-probe method, we can simultaneously obtain the two pulses with duration below 10 fs, which combines the ultrashort dual-color laser pulses.

4. Discussion

When a laser pulse interacts with atomic gases, the induced SPM effect achieves the spectral broadening and imparts a positive chirp on the pulse. For different requirements of input pulse energies and gas pressures, we will choose a suitable gas to compress the pulse based on its ionization potential and nonlinear refractive index. Generally, the Kr gas is used when the initial pulse energy is low due to the high nonlinear refractive index, while for intense pulse, we usually employ the Ne gas to compress the pulse because of its

high ionization potential. Therefore, a HCF compressor filled with atomic gases is the common tool to obtain the few-cycle pulses with micro- or millijoule energies. However, when this method is applied to the intense pulse, the phase becomes more complicated and its compensation is difficult, which restricts the pulse quality and even causes the pulse breakup.

For molecular gases, there is a rotational effect when interacting with an optical pulse. Based on the MPM effect induced by molecular rotations, we can obtain the few-cycle pulses with frequency tuning. This method has several desirable characteristics. First, it allows for some tunability of the compressed pulse; second it can impart a positive or negative chirp on the probe pulse, which means we can use the popular glasses to compensate the pulse instead of chirped mirrors; then the compressed pulse presents a smooth spectrum without modulation and promises a clean pulse profile. But this approach is limited by the intensity of probe pulse. The intense pulse will induce the enhanced SPM effect, which suppresses the pulse quality.

5. Conclusion

In summary, we have theoretically studied and compared the two pulse compression methods for generation of the few-cycle laser pulses in HCF filled with atomic or molecular gases. Based on SPM effect, the HCF compressor filled with noble gases is a widely used approach to obtain the few-cycle pulses with micro- or millijoule energies. With MPM effect, we focus on the extensive study of the SPM effect influence on the probe pulse and obtain the frequency-tunable few-cycle pulses only using the common glasses to compensate. Using the double pump-probe method, we also obtain the two few-cycle pulses, which can be used to combine the dual-color pulses and are promising as a tunable source.

References

[1] Zhou J, Peatross J, Murnane M M, Kapteyn H C and Christov I P 1996 *Phys. Rev. Lett.* **76** 752
[2] Scrinzi A, Ivanov M Y, Kienberger R and Villeneuve D M 2006 *J. Phys. B* **39** R1
[3] Krausz F and Ivanov M 2009 *Rev. Modern Phys.* **81** 163
[4] Zewail A H 1988 *Science* **242** 1645
[5] Suzuki T, Minemoto S, Kanai T and Sakai H 2004 *Phys. Rev. Lett.* **92** 133005
[6] Liu Y, Liu X, Deng Y, Wu C, Jiang H B and Gong Q H 2011 *Phys. Rev. Lett.* **106** 073004
[7] Nisoli M, Silvestri S D and Svelto O 1996 *Appl. Phys. Lett.* **68** 2793
[8] Nisoli M, Silvestri S D, Svelto O, Szipocs R, Ferencz K, Spielmann C, Sartania S and Krausz F 1997 *Opt. Lett.* **22** 522
[9] Chen X W, Jullien A, Malvache A, Canova L, Borot A, Trisorio A, Durfee C G and Lopez-Martens R 2009 *Opt. Lett.* **34** 1588
[10] Bohman S, Suda A, Kanai T, Yamaguchi S and Midorikawa K 2010 *Opt. Lett.* **35** 1887
[11] Klenke A, Kienel M, Eidam T, Hadrich S, Limpert J and Tunnermann A 2013 *Opt. Lett.* **38** 4593
[12] Jacqmin H, Jullien A, Mercier B, Hanna M, Druon F, Papadopoulos D and Lopez-Martens R 2015 *Opt. Lett.* **40** 709
[13] Zhu J F, Wang P, Han H N, Teng H and Wei Z 2008 *Sci. China Phys. Mech.* **51** 507
[14] Wittmann M, Nazarkin A and Korn G 2000 *Phys. Rev. Lett.* **84** 5508
[15] Bartels R A, Weinacht T C, Wagner N, Baertschy M, Greene C H, Murnane M M and Kapteyn H C 2001 *Phys. Rev. Lett.* **88** 013903
[16] Zhavoronkov N and Korn G 2002 *Phys. Rev. Lett.* **88** 203901
[17] Kalosha V, Spanner M, Herrmann J and Ivanov M 2002 *Phys. Rev. Lett.* **88** 103901
[18] Zhong F, Jiang H B and Gong Q H 2009 *Opt. Express* **17** 1472
[19] Wang F, Jiang H B and Gong Q H 2012 *J. Opt. Soc. Am. B* **29** 232
[20] Cai H, Wu J, Couairon A and Zeng H P 2009 *Opt. Lett.* **34** 827
[21] Bustard P J, Sussman B J and Walmsley I A 2010 *Phys. Rev. Lett.* **104** 193902
[22] Li M, Pan H, Tong Y, Chen C, Shi Y, Wu J and Zeng H P 2011 *Opt. Lett.* **36** 3633
[23] Wang F, Jiang H B and Gong Q H 2014 *Chin. Phys. B* **23** 014201
[24] Huang Z Y, Wang D, Leng Y X and Dai Y 2015 *Phys. Rev. A* **91** 043809
[25] Huang Z Y, Wang D, Leng Y X and Dai Y 2015 *Opt. Express* **23** 17711
[26] Courtois C, Couairon A, Cros B, Marques J R and Matthieussent G 2001 *Phys. Plasmas* **8** 3445
[27] Huang Z Y, Leng Y X and Dai Y 2014 *Chin. Phys. B* **23** 124210
[28] Huang Z Y, Wang D, Leng Y X and Dai Y 2015 *Chin. Phys. B* **24** 014212
[29] Bergé L, Skupin S, Nuter R, Kasparian J and Wolf J P 2007 *Rep. Prog. Phys.* **70** 1633
[30] Nubling R K and Harrington J A 1998 *Opt. Eng.* **37** 2454
[31] Pinault S C and Potasek M J 1985 *J. Opt. Soc. Am. B* **2** 1318
[32] Agrawal G P 2007 *Nonlinear Fiber Optics* (New York) p. 65
[33] Wang Y, Dai X, Wu J, Ding L and Zeng H P 2010 *Appl. Phys. Lett.* **96** 031105
[34] Huang Z Y, Wang D, Leng Y X and Dai Y 2015 *Chem. Phys. Lett.* **627** 53
[35] Wu J, Cai H, Couairon A and Zeng H P 2009 *Phys. Rev. A* **79** 063812